SciFed Publishers

SciFed Journal of Biofuel and Bioenergitcs

Research Article Open Access

On Similarity of Differential Capacity and Capillary Pressure Fractal Dimensions for Characterizing Shajara Reservoirs of the Permo-Carboniferous Shajara Formation, Saudi Arabia

*Khalid Elyas Mohamed Elameen AlKhidir

*Professor, Department of Petroleum and Natural Gas Engineering, College of Engineering, King Saud University, Saudi Arabia

Abstract

The quality of a reservoir can be described in details by the application of differential capacity. The objective of this research is to calculate fractal dimension from the relationship among differential capacity, maximum differential capacity and wetting phase saturation and to confirm it by the fractal dimension derived from the relationship among capillary pressure and wetting phase saturation. In this research, porosity was measured on real collected sandstone samples and permeability was calculated theoretically from capillary pressure profile measured by mercury intrusion techniques. Two equations for calculating the fractal dimensions have been used. The first one describes the functional relationship between wetting phase saturation, differential capacity, maximum differentia capacity and fractal dimension. The second equation implies to the wetting phase saturation as a function of capillary pressure and the fractal dimension. Two procedures for obtaining the fractal dimension have been developed. The first procedure was done by plotting the logarithm of the ratio between differential capacity and maximum differential capacity versus logarithm wetting phase saturation. The slope of the first procedure = 3- Df (fractal dimension). The second procedure for obtaining the fractal dimension was completed by plotting the logarithm of capillary pressure versus the logarithm of wetting phase saturation. The slope of the second procedure = Df -3. On the basis of the obtained results of the constructed stratigraphic column and the acquired values of the fractal dimension, the sandstones of the Shajara reservoirs of the Shajara Formation were divided here into three units. The gained units from bottom to top are: Lower Shajara differential capacity Fractal Dimension Unit, Middle Shajara differential capacity Fractal dimension Unit, and Upper Shajara differential capacity Fractal Dimension Unit. The results show similarity between differential capacity fractal dimension and capillary pressure fractal dimension. It was also noted that samples with wide range of pore radius were characterized by high values of fractal dimension due to an increase in their flow capacity. In our case, and as conclusions the higher the fractal dimension, the higher the permeability, the better the reservoir characteristics.

Keywords

Shajara Reservoirs; Shajara Formation; Differential Capacity Fractal Dimension; Capillary Pressure Fractal Dimension

Introduction

Capillary pressure is generally expressed as an aspect of the wetting phase saturation, according to the capillary pressure model [1]. The capillary pressure function was modified by Brooks RH and Corey AT [2] by applying a pore size distribution index (λ) as an exponent on the ratio of bubble pressure to capillary pressure. According to their results, a linear relationship exists between pressure and effective saturation on a log-log plot. This mathematical relationship has been named the

***Corresponding author:** Khalid Elyas Mohamed Elameen AlKhidir, Professor, Department of Petroleum and Natural Gas Engineering, College of Engineering, King Saud University, Saudi Arabia. E-mail: kalkhidir@KSU.EDU.SA; Tel: +966 11 4679118

Received August 30, 2018; **Accepted** September 04, 2018; **Published** September 17, 2018

Citation: Khalid Elyas Mohamed Elameen AlKhidir (2018) On Similarity of Differential Capacity and Capillary Pressure Fractal Dimensions for Characterizing Shajara Reservoirs of the Permo-Carboniferous Shajara Formation, Saudi Arabia. SF J Biofuel Bioenerg 1:2.

Brooks-Corey model (B-C model). A model that predicts the hydraulic conductivity for un- saturated soil-water retention curve and conductivity saturation was derived by Mualem YA [3]. Later, based on Mualem's formula, Van Genuchten MTh [4] described a relatively simple expression for the hydraulic conductivity of unsaturated soils. The Van Genuchten model (V-G model) contained three independent parameters, which can be obtained by fitting experimental data. A function to estimate the relationship between water saturation and capillary pressure in porous media was proposed by Oostrom M and Lenhard RJ [5]. This function is test data of sandstone rocks and carbonate rocks with high permeability were described as a new capillary pressure expression [6].

A fractal approach can be used to model the pc measured with mercury intrusion in Geysers grey wacke rock; however, the B-C model could not be used, according to a study by Li [7]. Sub-sequently, a theoretical analysis using fractal geometry was conducted by Li K and Horne RN [8] to deduce the B-C model, which has always been considered as an empirical model. Subsequently, fractal modeling of porous media was used to develop a more generalized capillary pressure model was studied by Li K [9]. With the new model [9] also evaluated the heterogeneity of rocks [10]. Physical parameters of soils in term of fractal dimension were studied by Globus AM [11]. An increase of volumetric water content with increasing hydraulic conductivity was reported by Alfaro Soto MA, et al. [12]. Bimodal Pore Size behavior of the Shajara Formation reservoirs of the permo-carboniferous Unayzah group was studied [13]. Subdivision of the Shajara reservoirs into three units based on thermodynamic fractal dimension approach and 3-D fractal geometry model of mercury intrusion technique was reported by Al-Khidir K, et al. [14]. The work published by Al-Khidir, et al. [14] was cited as Geoscience; New Finding reported from King Saud University Describe advances in Geoscience. Science Letter (Oct 25, 2013): 359. Al-khidir, et al. [15]. An increase of bubble pressure fractal dimension and pressure head fractal dimension with decreasing pore size distribution index and fitting parameters m×n due to possibility of having inter connected channels was proofed by Al-khidir KEME [16]. An increase of fractal dimension with increasing permeability, relaxation time of induced polarization, due to an increase in pore connectivity was confirmed by Alkhidir KEME [17].

Materials and Methods

Porosity was measured on collected sandstone samples and permeability was calculated from the measured capillary pressure by mercury intrusion techniques. Two procedures for obtaining the fractal dimension have been developed. The first procedure was concluded by plotting the logarithm of the ratio between differential capacity and maximum differential capacity versus logarithm wetting phase saturation. The slope of the first procedure = 3- Df (fractal dimension). The second procedure for obtaining the fractal dimension was resolved by plotting the logarithm of capillary pressure versus the logarithm of wetting phase saturation. The slope of the second procedure = Df -3.

The differential capacity can be scaled as

$$\mathbf{Sw} = \left[\frac{\mathbf{C}^{\frac{1}{2}}}{\mathbf{C}_{\max}^{\frac{1}{2}}} \right]^{[3-\mathbf{Df}]} \qquad (1)$$

Where Sw the water saturation, C the differential capacity in square meter, C_{max} the maximum differential capacity in square meter, and Df the fractal dimension.

Equation 1 can be proofed from

$$\boldsymbol{\varepsilon f} = \left[\frac{\mathbf{Q}}{\mathbf{V} * \mathbf{L}} \right] \qquad (2)$$

Where εf the permittivity of the fluid in faraday / meter, Q the electric charge in coulomb, V the electric potential in volt, and L the length in meter.

The electric charge can be scaled as

$$\mathbf{Q} = \left[\frac{\mathbf{vol}}{\mathbf{C_S}} \right] \qquad (3)$$

Where Q the electric charge in coulomb, vol the volume of the fluid in cubic meter, and C_S the streaming potential coefficient in volt / pascal.

Insert equation 3 into equation 2

$$\boldsymbol{\varepsilon f} = \left[\frac{\mathbf{vol}}{\mathbf{C_S} * \mathbf{V} * \mathbf{L}} \right] \qquad (4)$$

The volume can be scaled as

$$\mathbf{Vol = C * H} \qquad (5)$$

Where vol the volume of the fluid in cubic meter, C the differential capacity in square meter, and H the pressure head in meter

Insert equation 5 into equation 4

$$\varepsilon f = \left[\frac{C * H}{C_S * V * L}\right] \qquad (6)$$

The streaming potential coefficient can be scaled as

$$C_S = \left[\frac{reff^2 * C_E}{8 * \sigma f * \eta f}\right] \qquad (7)$$

Where Cs the streaming potential coefficient in volt / pascal, reff the effective pore radius in meter, C_E the electro osmosis coefficient in pascal / volt, σf the fluid conductivity in Siemens / meter, and ηf the fluid viscosity in pascal * second.

Insert equation 7 into equation 6

$$\varepsilon f = \left[\frac{C * H * 8 * \sigma f * \eta f}{reff^2 * C_E * V * L}\right] \qquad (8)$$

If the pore radius r in meter is introduced equation 8 will become

$$r^2 = \left[\frac{C * H * 8 * \sigma f * \eta f}{\varepsilon f * C_E * V * L}\right] \qquad (9)$$

The maximum pore radius can be scaled as

$$r_{max}^2 = \left[\frac{C_{max} * H * 8 * \sigma f * \eta f}{\varepsilon f * C_E * V * L}\right] \qquad (10)$$

Divide equation 9 by equation 10

$$\left[\frac{r^2}{r_{max}^2}\right] = \left[\frac{\left[\frac{C * H * 8 * \sigma f * \eta f}{\varepsilon f * C_E * V * L}\right]}{\left[\frac{C_{max} * H * 8 * \sigma f * \eta f}{\varepsilon f * C_E * V * L}\right]}\right] \qquad (11)$$

Equation 11 after simplification will become

$$\left[\frac{r^2}{r_{max}^2}\right] = \left[\frac{C}{C_{max}}\right] \qquad (12)$$

Take the square root of equation 12

$$\sqrt{\left[\frac{r^2}{r_{max}^2}\right]} = \sqrt{\left[\frac{C}{C_{max}}\right]} \qquad (13)$$

Equation 13 after simplification will become

$$\left[\frac{r}{r_{max}}\right] = \left[\frac{C^{\frac{1}{2}}}{C_{max}^{\frac{1}{2}}}\right] \qquad (14)$$

Take the logarithm of equation 14

$$\log\left[\frac{r}{r_{max}}\right] = \log\left[\frac{C^{\frac{1}{2}}}{C_{max}^{\frac{1}{2}}}\right] \qquad (15)$$

$$\mathbf{But;} \log\left[\frac{r}{r_{max}}\right] = \frac{\log Sw}{[3 - Df]} \qquad (16)$$

Insert equation 16 into equation 15

$$\frac{\log Sw}{[3 - Df]} = \log\left[\frac{C^{\frac{1}{2}}}{C_{max}^{\frac{1}{2}}}\right] \qquad (17)$$

Equation 17 after log removal will become

$$Sw = \left[\frac{C^{\frac{1}{2}}}{C_{max}^{\frac{1}{2}}}\right]^{[3-Df]} \qquad (18)$$

Equation 18 the proof of equation 1 which relates the water saturation, differential capacity, maximum differential capacity, and the fractal dimension.

The capillary pressure can be scaled as

$$\mathbf{Sw = [Df - 3] * Pc + constant} \qquad (19)$$

Results and Discussion

Based on field observation the Shajara Reservoirs of the Permo- Carboniferous Shajara Formation were divided here into three units as described in (Figure 1). These units from bottom to top are: Lower, Middle and Upper Shajara Reservoir. Their developed results of differential capacity

and capillary fractal dimensions are presented in (Table 1). The results display equalities between differential capacity fractal dimension and capillary pressure fractal dimension. A maximum fractal dimension value of about 2.7872 was informed from sample SJ13 as validated in (Table 1). But, a minimum fractal dimension value 2.4379 assigns to sample SJ3 from the Lower Shajara Reservoir as verified in (Table 1). The differential capacity and capillary pressure fractal dimensions were noticed to increase with increasing permeability due to the possibility of having interconnected channels as confirmed in (Table1). Regarding the Lower Shajara Reservoir, it is represented by six sandstone samples as shown in (Figure 1), four of which marked as SJ1, SJ2, SJ3, and SJ4 were taken for capillary pressure measurements to evaluate the fractal dimension. Their positive slopes of the first procedure (log ratio of differential capacity to maximum differential capacity versus log water saturation (Sw) and negative slopes of the second procedure (log capillary pressure (Pc) versus log water saturation (Sw) were designated in (Figures 2, 3, 4, 5 and Table 1). Their differential capacity fractal dimension and capillary pressure fractal dimension values are displayed in Table 1. As we proceed from sample SJ2 to SJ3 a remarkable reduction in permeability from 1955 md to 56 md was observed due to compaction which reveals change in differential capacity fractal dimension from 2.7748 to 2.4379 as explained in (Table 1). Such extreme change in permeability can account for heterogeneity which is a key parameter in reservoir quality assessment. Once more, an increase in grain size and permeability was informed from sample SJ4 whose differential capacity fractal dimension and capillary pressure fractal dimension was found to be 2.6843 as illustrated in (Table 1).

Figure 1: Surface Type Section of the Shajara Reservoirs of the Permo-Carboniferous Shajara Formation, Latitude 26 52 17.4, Longitude 43 36 18

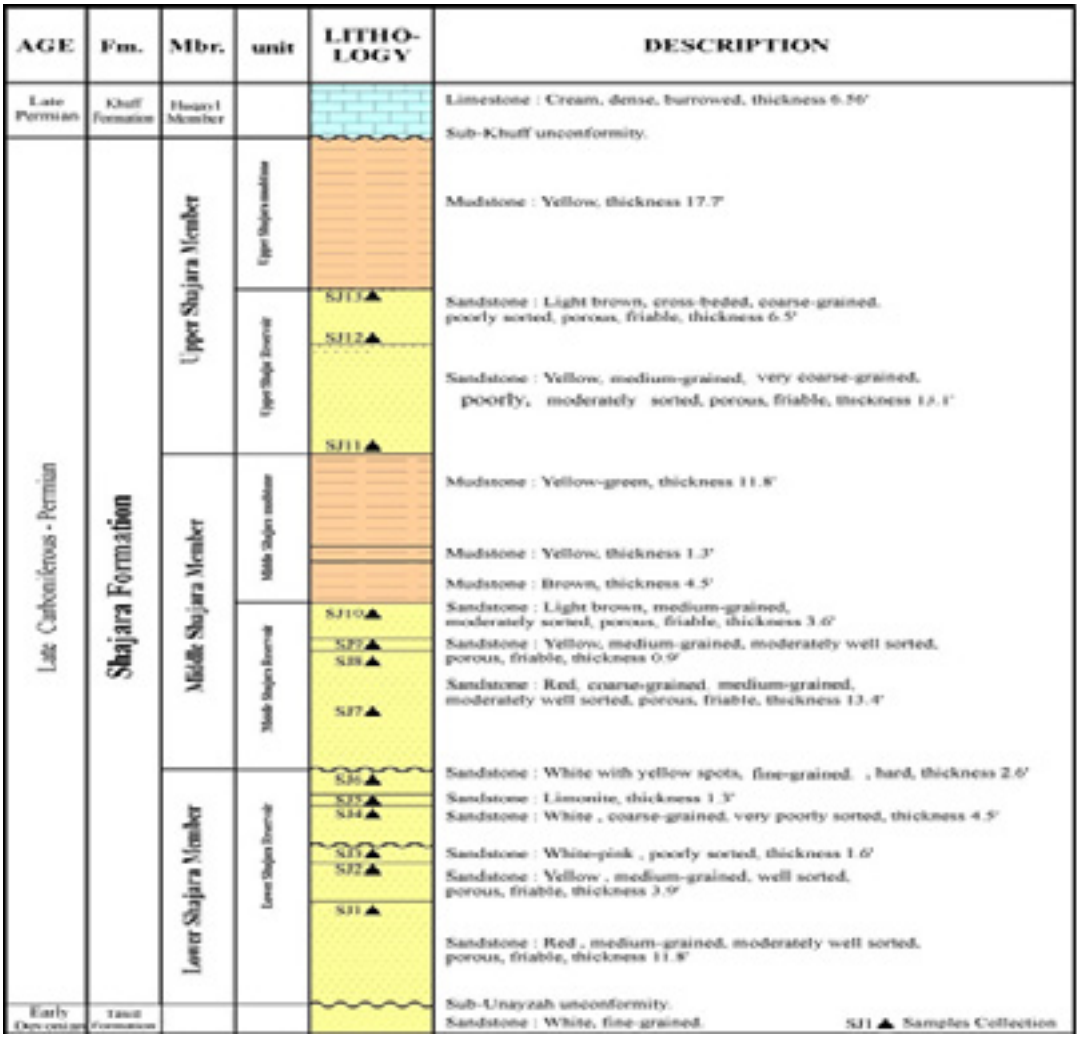

Figure 2: Log ($C^{1/2}/C_{max}^{1/2}$) & log Pc Versus log Sw for Sample SJ1

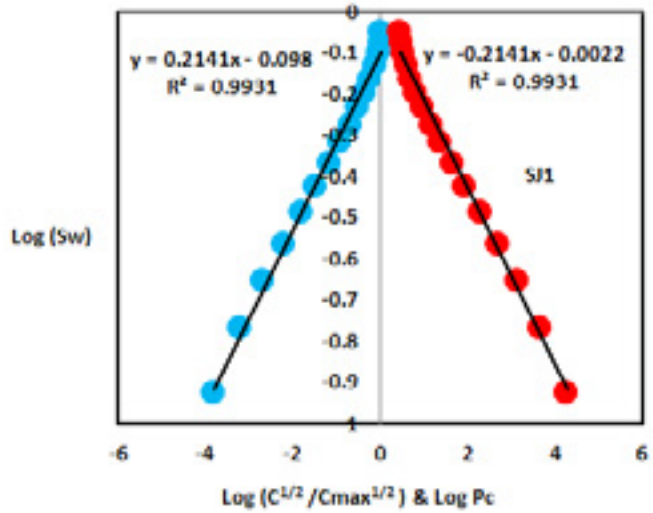

Figure 3: Log ($C^{1/2}/C_{max}^{1/2}$) & log Pc Versus log Sw for Sample SJ2

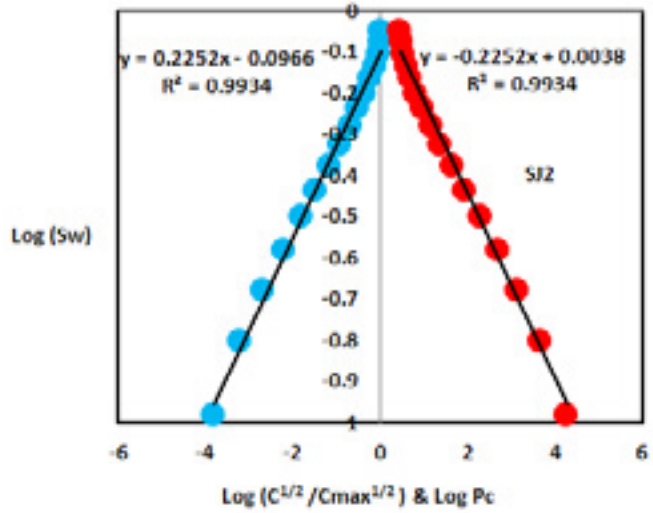

Figure 4: Log ($C^{1/2}/C_{max}^{1/2}$) & log Pc Versus log Sw for Sample SJ3

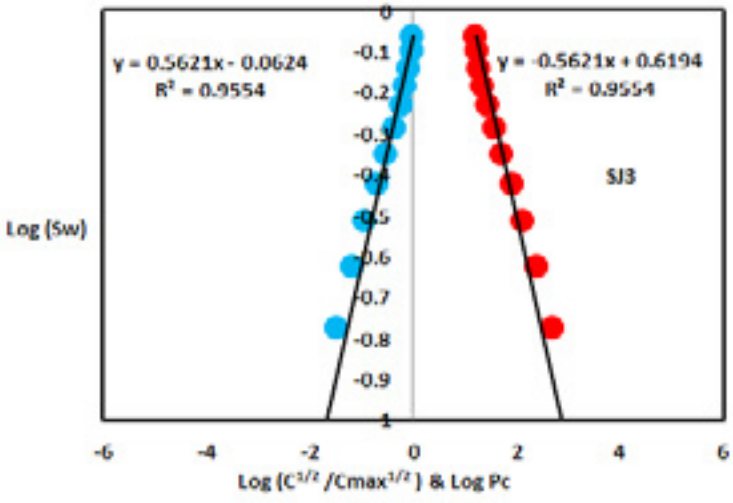

Figure 5: Log ($C^{1/2}/C_{max}^{1/2}$) & log Pc Versus log Sw for Sample SJ4

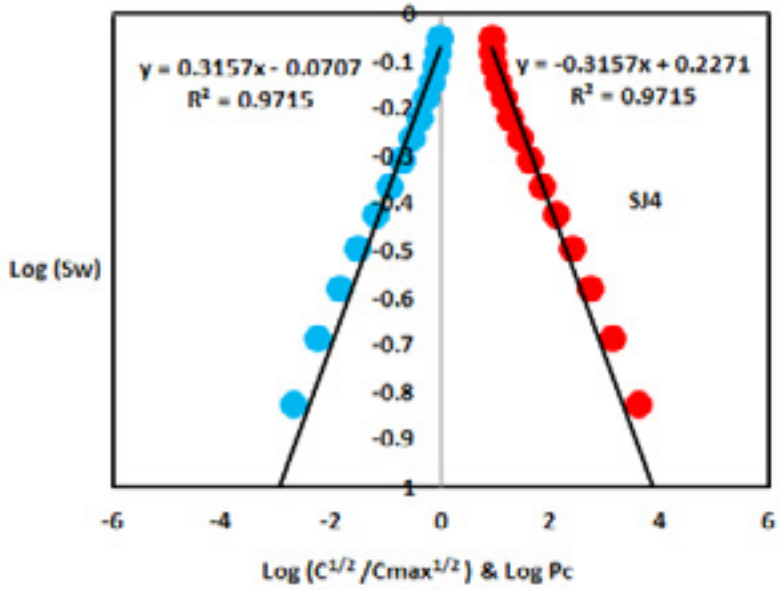

Table 1: Petrophysical Model showing the Three Shajara Reservoir Units with their Corresponding Values of Differential Capacity Fractal Dimension and Capillary Pressure Fractal Dimension

Formation	Reservoir	Sample	Porosity %	k (md)	Positive Slope of the First Procedure Slope=3-Df	Negative Slope of the Second Procedure Slope=Df-3	Differential Capacity Fractal Dimension	Capillary Pressure Fractal Dimension
Permo-Carboniferous Shajara Formation	Upper Shajara Reservoir	SJ13	25	973	0.2128	-0.2128	2.7872	2.7872
		SJ12	28	1440	0.2141	-0.2141	2.7859	2.7859
		SJ11	36	1197	0.2414	-0.2414	2.7586	2.7586
	Middle Shajara Reservoir	SJ9	31	1394	0.2214	-0.2214	2.7786	2.7786
		SJ8	32	1344	0.2248	-0.2248	2.7752	2.7752
		SJ7	35	1472	0.2317	-0.2317	2.7683	2.7683
	Lower Shajara Reservoir	SJ4	30	176	0.3157	-0.3157	2.6843	2.6843
		SJ3	34	56	0.5621	-0.5621	2.4379	2.4379
		SJ2	35	1955	0.2252	-0.2252	2.7748	2.7748
		SJ1	29	1680	0.2141	-0.2141	2.7859	2.7859

Concerning the Middle Shajara Reservoir, it is separated from Lower Shajara Reservoir by an unconformity surface as described in (Figure 1). It was signified by four samples, three of which named as SJ7, SJ8, and SJ9 were selected for fractal dimension determination as proved in (Table 1). Their positive and negative slopes of the first and second procedures were defined in (Figures 6, 7, 8 and Table 1) Furthermore, their differential capacity and capillary pressure fractal dimension shows equal values as presented in (Table 1) Likewise, their fractal dimension values are higher than those of sample SJ3 and SJ4 from the Lower Shajara Reservoir due to an increase in their permeability as identified in (Table 1). On the other hand, the Upper Shajara reservoir is separated from the Middle Shajara reservoir by yellow green mudstone as shown in (Figure 1). It is defined by three samples so called SJ11, SJ12, SJ13 as explained in (Table 1). Their positive slopes of the first procedure and negative slopes of the second procedure are displayed in (Figures 9, 10, 11 and Table 1). Also, their differential capacity fractal dimension and capillary pressure fractal dimension are also higher than those of sample SJ3 and SJ4 from the Lower Shajara Reservoir due to an increase in their permeability as testified in (Table 1). Global a plot of positive slope of

the first procedure versus negative slope of the second procedure delineates three reservoir zones of varying petrophysical characteristics as shown in (Figure 12). These zones were also confirmed by plotting differential capacity fractal dimension versus capillary pressure fractal dimension as shown in (Figure 13). Such variation in fractal dimensions can be used to explain heterogeneity which is a key parameter in reservoir quality assessment.

Figure 6: Log ($C^{1/2}/C_{max}^{1/2}$) & log Pc Versus log Sw for Sample SJ7

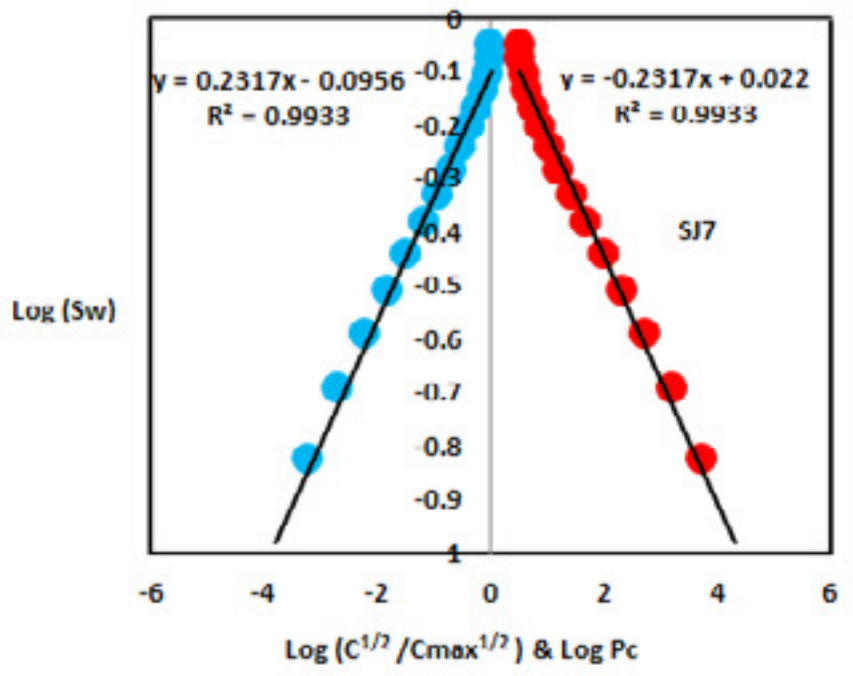

Figure 7: Log ($C^{1/2}/C_{max}^{1/2}$) & log Pc Versus log Sw for Sample SJ8

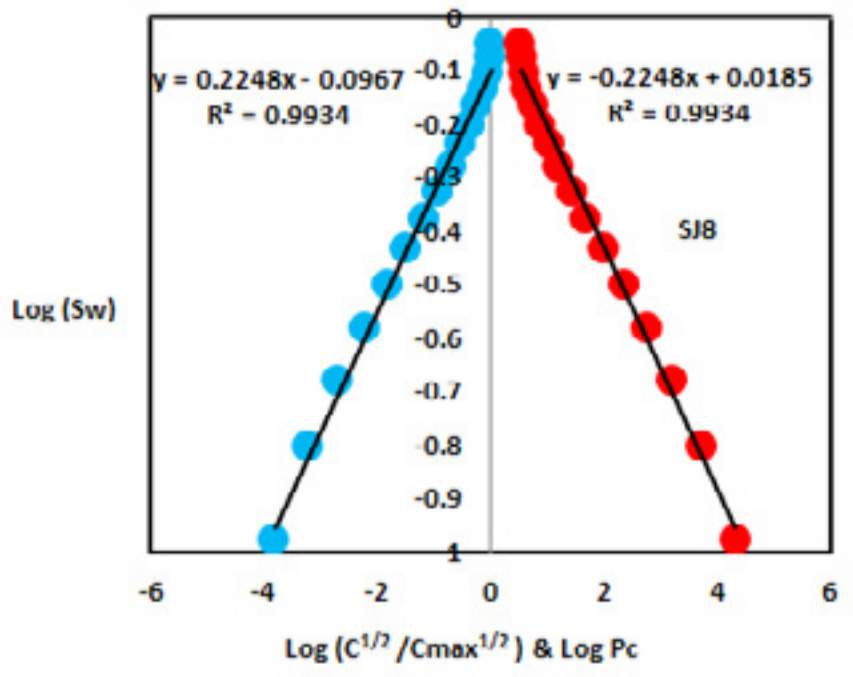

Figure 8: Log ($C^{1/2}/C_{max}^{1/2}$) & log Pc Versus log Sw for Sample SJ9

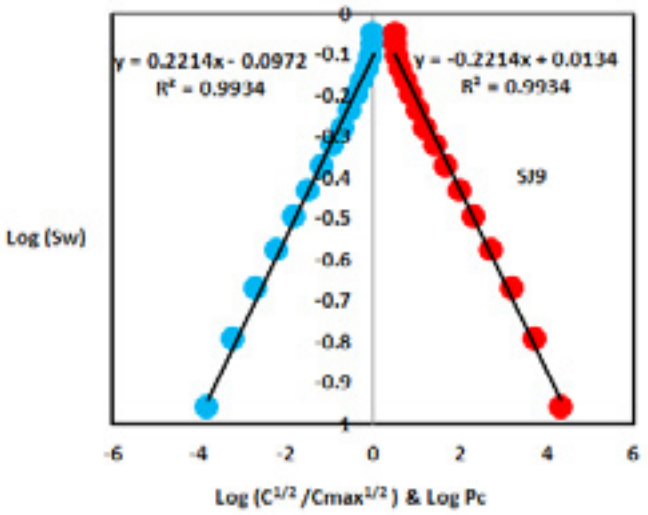

Figure 9: Log ($C^{1/2}/C_{max}^{1/2}$) & log Pc Versus log Sw for Sample SJ11

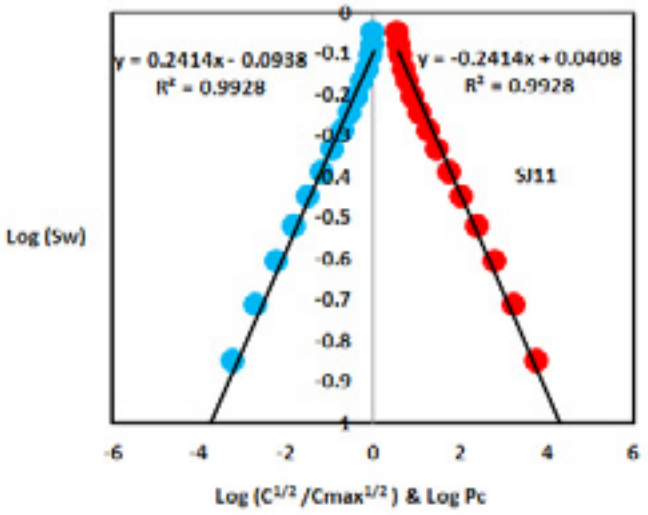

Figure 10: Log ($C^{1/2}/C_{max}^{1/2}$) & log Pc Versus log Sw for Sample SJ12

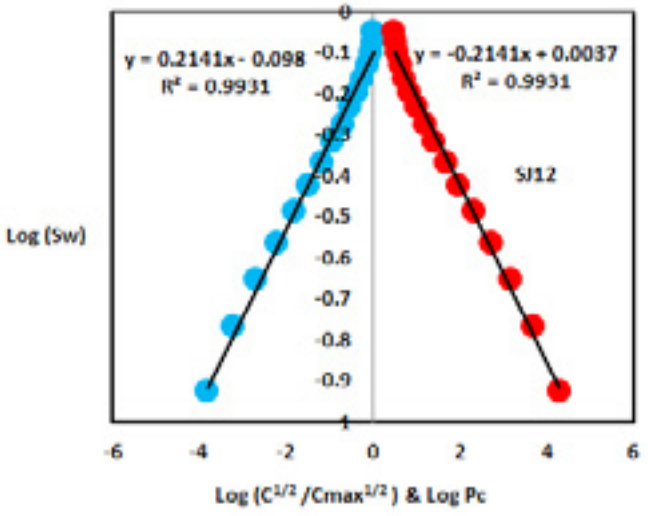

Figure 11: Log ($C^{1/2}/C_{max}^{1/2}$) & log Pc Versus log Sw for Sample SJ13

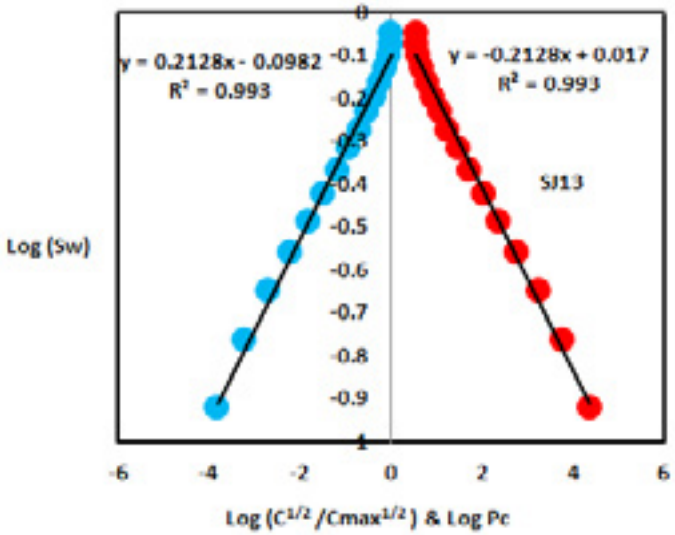

Figure 12: Positive Slope of the First Procedure Versus Negative Slope of the Second Procedure

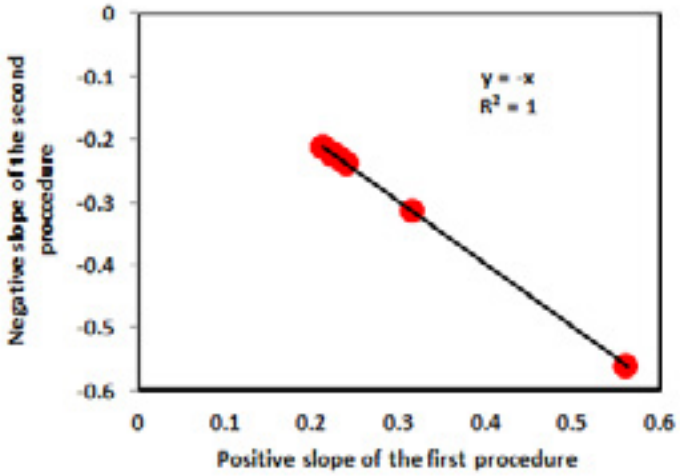

Figure 13: Differential Capacity Fractal Dimension Versus Capillary Pressure Fractal Dimension

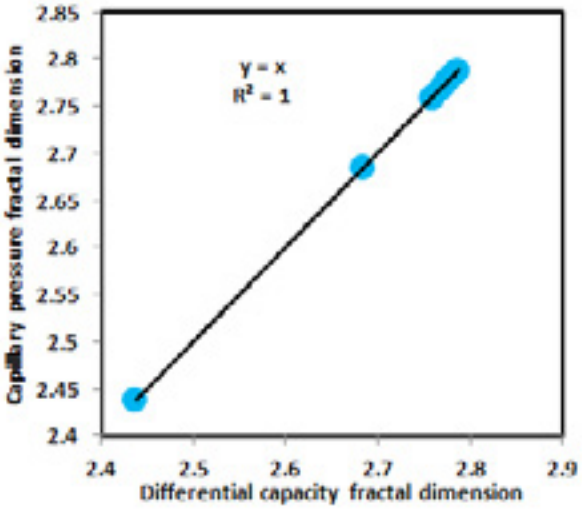

References

1. Leverett MC (1941) Capillary Behavior in Porou Solids. Trans AIME142 1: 152-169.

2. Brooks RH, Corey AT (1964) Hydraulic Properties of Porous Media. Hydrology Paper 3, Colorado State University, Fort Collins.

3. Mualem YA (1976) A New model for Predicting the Hydraulic Conductivity of Un- Saturated Porous Media. Water Resources Research 12: 513-522.

4. Van Genuchten MTh (1980) A Closed Form Equation for Predicting the Hydraulic Conductivity of Unsaturated Soils. Soil Sci Soc Am J 44: 892-898.

5. Oostrom M, Lenhard RJ (1998) Comparison of Relative Permeability. Saturation-Pressure Parametric Models for Infiltration and Redistribution of a Light Non-Aqueous Phase Liquid in Sandy Porous Media. Adv Water Resour 212: 145-157.

6. Jing XD, Van Wunnik JNM (1998) A Capillary Pressure Function for Interpretation of Core-Scale Displacement Experiments. 9807. Imperial College, SCA, UK 14-22.

7. Li K (2004) Generalized Capillary Pressure and Relative Permeability Model Inferred from Fractal Characterization of Porous Media. In: Proceedings of the Annual Technical Conference and Exhibition, Houston, Texas. Society of Petroleum Engineers 89874.

8. Li K, Horne RN (2006) Fractal Modeling of Capillary Pressure Curves for the Geysers Rocks. Geothermic 35: 198-207.

9. Li K (2010a) More General Capillary Pressure and Relative Permeability Models from Fractal Geometry. J Contam Hydrol 111: 13-24.

10. Li K (2010b) Analytical Derivation of Brooks-Corey Type Capillary. Pressure Models Using Fractal Geometry and Evaluation of Rock Heterogeneity. J Petrol Sci Eng 73: 20-26.

11. Globus AM (2006) Fractal Character of Some Physical Parameters of Soils. Eurasian Soil Science 39: 1116-1126.

12. Alfaro Soto MA, Chang HK, Van Genuchten MTh (2017) Fractal-based models for the unsaturated soil hydraulic functions. Geoderma 306: 144-151.

13. Al-Khidir KA, Al-Laboun A, Al-Qurishi A, et al. (2011) Bimodal Pore Size Behavior of the Shajara Formation Reservoirs of the Permo-Carboniferous Unayzah Group, Saudi Arabia. J Petroleum Exploration Production Technol 1: 1-9.

14. Al-Khidir K, Benzagouta M, Al-Qurishi A, et al. (2013) Characterization of Heterogeneity of the Shajara Reservoirs of the Shajara Formation of the Permo-Carboniferous Unayzah Group. Arab J Geosci 6: 3989-3995.

15. Al-Khidir (2013) Geoscience; New Findings Reported from King Saud 13. University Describe Advances in Geoscience Science Letter 359.

16. Al-khidir KEME (2017) Pressure head fractal dimension for characterizing Shajara reservoirs of the Shajara formation of the permo-Carboniferous Unayzah group, Saudi Arabia. Arch Petroleum Environ Biotechnol 1-7.

17. Alkhidir KEME (2018) Geometric relaxation time of induced polarization fractal dimension for characterizing Shajara reservoirs of the Shajara formation of the Permo-Carboniferous Unayzah group. Saudi Arabia. SF J Petroleum 2: 1-6.

Citation: Khalid Elyas Mohamed Elameen AlKhidir (2018) On Similarity of Differential Capacity and Capillary Pressure Fractal Dimensions for Characterizing Shajara Reservoirs of the Permo-Carboniferous Shajara Formation, Saudi Arabia. SF J Biofuel Bioenerg 1:2.